INTERNATIONAL JOURNAL FOR NUMERICAL METHODS IN FLUIDS
Int. J. Numer. Meth. Fluids 2005; **48**:1241–1257
Published online 19 May 2005 in Wiley InterScience (www.interscience.wiley.com). DOI: 10.1002/fld.990

Contrasting a novel temporally orientated Hamilton–Jacobi-equation-based ILES method with other approaches for a complex geometry flow

P. G. Tucker*,† and Y. Liu‡

Civil and Computational Engineering Centre, School of Engineering, University of Wales, Singleton Park, Swansea SA2 8PP, U.K.

SUMMARY

Flow and heat transfer inside an idealized electronics system is simulated using large-eddy simulation (LES)-related approaches that have been validated for simpler canonical flows. These include: Yoshizawa LES, detached eddy simulation (DES), limited numerical scales (LNS) and other hybrid LES–RANS (Reynolds-averaged Navier–Stokes) approaches including a new ILES (implicit LES)–RANS method. For the ILES, dissipation from the one legged temporal discretization is used to drain turbulence. The use of differential equations, including the Hamilton–Jacobi and Eikonal, to model turbulence distance functions is explored. The Hamilton–Jacobi is shown to be especially compatible with the zonal RANS–ILES approach and the Eikonal with DES. Performances of the LES-related methods are compared with explicit algebraic stress unsteady RANS (URANS) results and also measurements. Considering the problem complexity, generally, for all methods, predicted mean velocities and turbulence intensities are in a reasonable agreement with measurements. Average errors are 15 and 25%, respectively. With the exception of the zonal ILES–RANS method, turbulence intensities are underpredicted. For heat transfer, none of the models performs well giving circa 100% errors. Notably, the LNS performs poorly for both the flow field and heat transfer giving a highly complex RANS–LES interface with inappropriate upstream LES boundary conditions. DES is found impossible to converge. This is partly attributed to the irregular LES–RANS interface arising with the method. All the LES approaches significantly underpredict heat transfer and the URANS over-predicts. Even the increased flow activity arising from use of the less dissipative ILES element does not prevent the significant heat transfer under-prediction. Copyright © 2005 John Wiley & Sons, Ltd.

KEY WORDS: LES; hybrid LES–RANS; Hamilton–Jacobi equation; one legged temporal discretization; ILES; URANS; heat transfer; electronics

*Correspondence to: P. G. Tucker, Civil and Computational Engineering Centre, School of Engineering, University of Wales, Singleton Park, Swansea SA2 8PP, U.K.
†E-mail: p.g.tucker@swansea.ac.uk
‡E-mail: y.liu@swansea.ac.uk

Contract/grant sponsor: EPSRC; contract/grant number: GR/N05581

Received 19 November 2004
Revised 6 April 2005
Accepted 11 April 2005

1. INTRODUCTION

With ever-increasing power densities the reliable prediction of fluid flow and heat transfer in electronics is becoming especially important. In reality, the flow inside most electronic systems is turbulent and due to the geometrical complexity also can exhibit large-scale, more coherent, unsteadiness. Present-day useable turbulence modelling techniques for industrial applications involve Reynolds-averaged Navier–Stokes (RANS) or unsteady RANS (URANS). To a much lesser extent pure large-eddy simulation (LES) and blends of LES and (U)RANS can be used. In (U)RANS, the Navier–Stokes equations (NSE) are essentially, in theory, time averaged to remove higher frequency temporal components and Lagrangian spatial scales associated with turbulence. Hence, flow solutions have a more regular smoother appearance. In contrast to the (U)RANS, in LES the NSE are spatially filtered. Eddies smaller than a characteristic resolution Δ (typically defined by grid spacing), known as sub-grid scales (SGS), are filtered out and hence need to be modelled. Eddies larger than Δ are resolved. Since most turbulence is resolved and not subjected to the vagaries of modelling, LES is capable of capturing unsteady flow feature better than (U)RANS and can give more accurate solutions.

Despite LES being superior to URANS, it still has some theoretical and practical drawbacks (see References [1, 2]) such as high computational cost for wall-bounded flows. An alternative to LES is the monotonically integrated LES (MILES) or ILES introduced by Boris *et al.* [1]. In ILES, monotone higher order convection or other algorithms are used to discretize the unfiltered NSE. These algorithms can, through numerical dissipation (and other properties), produce a built-in filter and a corresponding implicit SGS model. Grinstein and Fureby [2] demonstrate that ILES can be successfully used to simulate a wide range of flows and owing to the absence of sub-grid stress term calculations, can also lead to substantial savings in computational effort. Although ILES has some theoretical justification from a pragmatic viewpoint it is likely that in most industrially related LES-type simulations the numerical dissipation (which can arise through many sources including lack of preconditioning in certain types of flow solvers) takes on a greater role than that implied by the SGS model. Under these circumstances it appears most sensible to improve solution accuracy by switching the SGS model (which often has uncertain applicability) off. It is in this spirit that the ILES is explored here. Of course the temporal rather than spatial discretization can be used to supply filtering/dissipation. Novel use of the former is tried here.

In addition to ILES, along different lines other approaches aimed at reducing LES computational costs are hybrid LES–RANS methods. The first of these, detached eddy simulation (DES), was proposed by Spalart *et al.* [3]. With this, to avoid the need for such fine grids, intricate, fine, anisotropic boundary layer features, requiring especially high resolution (for LES, flow aligned streak structures need a grid spacing of around 20 wall units), are (U)RANS modelled. However, the accuracy advantages of LES are utilized away from walls where structures are larger and less intricate. Broadly following this strategy, various combinations of RANS and LES models have been investigated (see References [4–6]). Notably, Tucker [7] produces hybrid ILES–RANS solutions. With this, the very different turbulence length scales implied by the RANS and ILES models are blended using a Hamilton–Jacobi (HJ) equation. It is worth noting here that LES strategies often also include a RANS element. For example, some LES practitioners express the modelled turbulence length scale as the $\min[\kappa d, \Delta]$ where κ is the Von Karman constant, d the normal wall distance and Δ a filter width. This results in a simple mixing length model near walls.

Essentially, another hybrid LES–RANS method is the limited numerical scales (LNS) approach proposed by Batten *et al.* [8] and inspired by Speziale [9]. The idea of LNS is to derive the SGS stress from the underlying Reynolds stress via a latency parameter, α, based on the ratio of products of turbulence length- and velocity-scales. When $\alpha = 1$, cubic non-linear RANS modelling is applied and when $\alpha < 1$, LES is used. This is an improvement on the idea of Speziale [9] which is theoretically flawed in switching directly from URANS to DNS (direct numerical simulation) with no LES range. Unlike other hybrid LES–RANS methods, in which RANS modelling is always used near walls and LES away from them, with LNS, depending on mesh resolution, RANS modelling or LES may occur anywhere. If the grid is LES sufficient LES will automatically be used. This is attractive since a program user does not have to be so concerned with traditional LES issues such as whether the grid has sufficient resolution to reach the inertial sub-range region.

This study considers the configuration shown in Figure 1, which represents an idealized central processor unit. Two fans drive the flow. By electronics system standards these fans are large and so give rise to a relatively high Reynolds number flow. To investigate heat transfer, a heater is mounted on one horizontal surface. Since the ratio of Gr/Re^2 (Gr and Re are the Grashof and Reynolds numbers, respectively) is low (<0.01), buoyancy forces can be neglected. Partly owing to the presence of blocks and grills, the Figure 1 geometry flow is expected to be complicated exhibiting transition from laminar to turbulent flow, unsteady separation, reattachment, strong streamline curvature and regions with impingement. Furthermore, it is expected that large coherent vortex structures will convect over the heated surface [10]. Also, there is a possibility of non-unique solutions (see References [11, 12]). In addition, the flow complexity makes construction of a grid where the cross-stream spacing is sufficient to resolve streaks challenging. This factor in part makes the current zonal studies sensible.

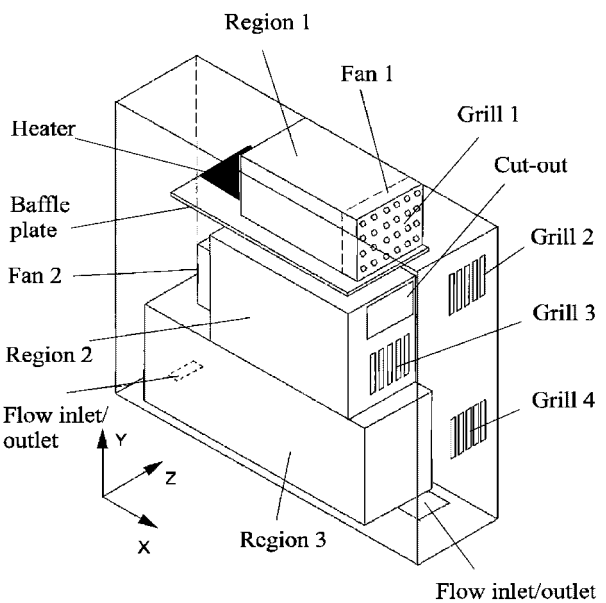

Figure 1. Schematic of an idealized system studied.

This paper extends previous (U)RANS [13, 14] studies of this unsteady complex geometry flow. The applicability of above-mentioned hybrid (I)LES–RANS, LNS and DES approaches is considered. To set the performances of these new models into context, results are compared with zonal k-l/EASM (explicit algebraic stress model [15]) URANS and Yoshizawa [16] LES results. Also, all results are compared with laser doppler anemometry (LDA) and new heat transfer measurements.

2. NUMERICAL METHOD

2.1. Governing equations

The following equations governing mass, momentum and energy conservation for incompressible flows are solved:

$$\frac{\partial \tilde{u}_j}{\partial x_j} = 0 \tag{1}$$

$$\rho \frac{\partial \tilde{u}_i}{\partial t} + \rho \frac{\partial (\tilde{u}_i \tilde{u}_j)}{\partial x_j} = -\frac{\partial \tilde{p}}{\partial x_i} + \frac{\partial}{\partial x_j}\left[\mu \frac{\partial \tilde{u}_i}{\partial x_j}\right] + \frac{\partial \tau_{ij}}{\partial x_j} \tag{2}$$

$$\rho \frac{\partial \tilde{T}}{\partial t} + \rho \frac{\partial (\tilde{u}_j \tilde{T})}{\partial x_j} = \frac{\partial}{\partial x_j}\left[\frac{\mu}{Pr} \frac{\partial \tilde{T}}{\partial x_j}\right] + \frac{\partial h_j}{\partial x_j} \tag{3}$$

The tilde is used to identify that variables can have dual physical contexts representing time-averaged or filtered (spatially averaged) values for URANS and (I)LES, respectively. In Equations (1)–(3), $\tilde{u}_i$ is a fluid velocity component ($i = 1, 2, 3$ corresponding to the x, y and z directions, respectively), ρ the fluid density, μ dynamic viscosity, $\tilde{p}$ static pressure, $\tilde{T}$ temperature and t time. Pr is the Prandtl number of the fluid. To close the above equations the stress tensor, τ_{ij}, in Equation (2) and heat flux tensor, h_{ij}, in Equation (3) need to be modelled.

2.2. LES/ILES

In conventional LES, for a SGS model based on the eddy viscosity, the SGS stress tensor, τ_{ij}, is defined as

$$\tau_{ij} = 2\mu_{\mathrm{SGS}} S_{ij} - \frac{\tau_{kk}}{3} \delta_{ij} \tag{4}$$

where μ_{SGS} is the SGS eddy viscosity, $S_{ij} = (\partial \tilde{u}_i/\partial x_j + \partial \tilde{u}_j/\partial x_i)/2$ is the strain rate tensor and δ_{ij} the Kronecker delta. Here for LES computations μ_{SGS} is evaluated from the Yoshizawa [16] model. This uses a transport equation for the sub-grid scale k, which takes the following form:

$$\rho \frac{\partial k}{\partial t} + \rho \frac{\partial \tilde{u}_j k}{\partial x_j} = \frac{\partial}{\partial x_j}\left[\left(\mu + \frac{\mu_{\mathrm{SGS}}}{\sigma_k}\right)\left(\frac{\partial k}{\partial x_j}\right)\right] + P_k - \rho\varepsilon \tag{5}$$

where $P_k = 2\mu_{SGS}S_{ij}S_{ij}$ and $\varepsilon = C_\varepsilon k^{1.5}/\Delta$. Δ is a cell-volume-based filter, i.e. $\Delta = (\Delta x \Delta y \Delta z)^{1/3}$. The value of constant C_ε is 1.05. In ILES context, although $\mu_{SGS} = 0$, an effective eddy viscosity can be produced by numerical diffusion.

2.3. Hybrid (I)LES–RANS

Broadly four hybrid (I)LES–RANS approaches are tried. These are DES, Tucker and Davidson's [6] k-l-based zonal LES (ZLES), zonal ILES [7] (temporally dissipated) and LNS. In Z(I)LES, the Wolfshtein [17] k-l RANS model is used near walls. Either the Yoshizawa LES or ILES is used for the core region. The interface between the RANS and (I)LES models is defined through the dimensionless wall distance (y^+_{int}). Results are compared when the wall shear stress used in y^+_{int} is spatially and temporally averaged ($y^+_{int,ave} = 30$) and also based on instantaneous local values ($y^+_{int} = 30$). For k-l/ILES, just $y^+_{int,ave} = 30$ is used and the wall distance is calculated using a HJ equation (see Equation (9)) [7]. The latter smoothly blends the dramatically different modelled turbulence length scales implied by the RANS and ILES modelling. For ZLES multigrid based smoothing operators [6] are used. For DES, near walls the Spalart–Allmaras [18] (S–A) (U)RANS model is used. Away from them essentially Smagorinsky [19] LES is applied. The interface between these zone is set at $y_{int} = 0.65\max(\Delta x, \Delta y, \Delta z)$ where the Δ terms are grid spacings. Clearly, the interface is grid controlled and this can create irregularities.

2.4. Limited Numerical Scales (LNS)

In Batten *et al.*'s [8] LNS method, the eddy viscosity takes the following form:

$$\mu_T = \alpha C^*_\mu f_\mu \rho \frac{k^2}{\varepsilon} \tag{6}$$

where α is the so-called latency parameter. This is defined as

$$\alpha = \min[(LV)_{LES}, (LV)_{RANS}]/(LV)_{RANS} \tag{7}$$

where $(LV)_{LES} = C_S(L^\Delta)^2|S|$ is the product of the LES length and velocity scales and $(LV)_{RANS} = \delta + C^*_\mu k^2/\varepsilon$ for RANS, in which the constant $C_s = 0.05$, $L^\Delta = 2\max[\Delta x, \Delta y, \Delta z]$, $|S| = \sqrt{2S_{ij}S_{ij}}$ and $\delta = 10^{-20}$. The form of the transport equation for k is the same as Equation (5), but μ_{SGS} is replaced by μ_T, $P_k = -\rho\overline{u'_i u'_j}\partial\tilde{u}_i/\partial x_j$ (the primes representing fluctuating components). The dissipation rate ε is evaluated by solving the following equation:

$$\rho\frac{\partial\varepsilon}{\partial t} + \rho\frac{\partial\tilde{u}_j\varepsilon}{\partial x_j} = \frac{\partial}{\partial x_j}\left[\left(\mu + \frac{\mu_T}{\sigma_\varepsilon}\right)\left(\frac{\partial\varepsilon}{\partial x_j}\right)\right] + (C_{\varepsilon 1}P_k - C_{\varepsilon 2} + E)T_t^{-1} \tag{8}$$

where E is a source term and $T_t = k\max(1, \sqrt{2/R_t})/\varepsilon$ is a realizable time scale. The Reynolds stress tensor, $-\rho\overline{u'_i u'_j}$, is computed from a cubic non-linear expression [8]. As to the definitions of C^*_μ, f_μ and other parameters also see Batten *et al.* [8]. As mentioned before, to large extent, the mesh used decides the model switch from RANS to LES or the reverse.

2.5. Wall distance function

Wall 'distances' $\tilde{d}$ (again the tilde highlights that a variable with two quite different contexts can be used) are either evaluated using Poisson [13], Eikonal or HJ equations. The HJ equation [7] is expressed as

$$|\nabla \tilde{d}| = 1 + f(\tilde{d})\nabla^2 \tilde{d} + g(d) \tag{9}$$

Here $f(d) = \varepsilon_0 \tilde{d}$ and $g(d) = \varepsilon_1 (d/L)^n$. The length scale L is the distance from walls to the ILES region and n is a positive integer. When $\varepsilon_0 = \varepsilon_1 = 0$, Equation (9) reduces to the hyperbolic natured Eikonal equation. Weak viscosity solutions of this give exact nearest wall distances $d = \tilde{d}$. The Eikonal equation can be solved by propagating fronts from solid surfaces [20]. Here, the equation is propagated towards the RANS/ILES interface. Then at the interface, the condition $d = 0$ is set and Equation (9) solved using a Newton approach with $\varepsilon_0, \varepsilon_1 \geqslant 0$. The Laplacian enables a smooth transition between the modelled RANS length scale (that needs an accurate d) and the ILES zone (needing $d = 0$). The function $f(\tilde{d})$ forces the Laplacian to tend to zero near walls. This ensures near wall distances are accurate. The function $g(d)$ controls the RANS length scale in the vicinity of the ILES zone. It governs the biasing of the $\tilde{d}$ maximum. Typical Equation (9) $\tilde{d}$ distributions for various ε_0 and ε_1 combinations can be found in Reference [7]. For DES $\tilde{d}$ is initialized as $0.65 \max(\Delta x, \Delta y, \Delta z)$. The front propagation naturally terminates at the RANS–LES interface creating a potentially economical ready to use DES distance scale field.

2.6. Heat flux modelling

The simple eddy diffusivity model is used in this study, which takes the following form:

$$h_j = \frac{\mu_T}{Pr_t} \frac{\partial \tilde{T}}{\partial x_j} \tag{10}$$

For URANS, $\mu_T = \mu_t$ (eddy viscosity) and the turbulent Prandtl number $Pr_t = 0.9$. For LES, $\mu_T = \mu_{\mathrm{SGS}}$ and $Pr_t = 0.4$. For ILES, $\mu_T = 0$.

2.7. Calculation of turbulence intensity and percentage errors

Conventionally, the turbulence intensity is defined as $T_i = u'/U$ (U—time-mean velocity in the x direction). Here, for LES-related zonal methods, modelled turbulence contributions are neglected and u' is obtained only from the resolved field. Therefore, T_i is given by

$$T_i = \frac{\sqrt{\langle \tilde{u}\tilde{u} \rangle - \langle \tilde{u} \rangle^2}}{\langle \tilde{u} \rangle} \tag{11}$$

where $\langle \bullet \rangle$ denotes a time-averaging operation. When comparing predictions with measurements, the following formulation is used to calculate percentage errors:

$$\mathrm{Error}_U = \frac{\sum_{i=1}^{m} |U_{\mathrm{exp}} - U_{\mathrm{num}}|}{\sum_{i=1}^{m} |U_{\mathrm{exp}}|}, \quad \mathrm{Error}_{Ti} = \frac{\sum_{i=1}^{m} |T_{i,\mathrm{exp}} - T_{i,\mathrm{num}}|}{\sum_{i=1}^{m} |T_{i,\mathrm{exp}}|} \tag{12}$$

where m is the total number of experimental points, and the subscripts, 'exp' and 'num', represent experimental data and numerical values, respectively. At points where numerical

data points do not coincide exactly with measurements, a stiff quadratic spline interpolation is used.

2.8. Boundary conditions and numerical details

For velocities, at solid surfaces the usual no-slip and impermeability conditions are applied. At inflow boundaries the total pressure is fixed, the normal velocity set to conserve mass and the remaining velocity components made zero. At flow outlets the pressure is fixed, the normal velocity again set to conserve mass and the gradients of all other variables set to zero in a second order fashion. Prior to the solution starting it is not known which are inflow and outflow boundaries. Therefore, the above boundary conditions are set automatically depending on the flow direction at each iteration.

The sensitivity of RANS predictions to assumed values of turbulence intensities at flow inlets is tested by varying the intensity between 0 and 10%. Profiles presented are found insensitive to this variation.

The slotted grills 1–4 are modelled using loss coefficients of the form

$$E_l = \tfrac{1}{2} K \rho U_j^2 \tag{13}$$

where E_l is the loss of energy per unit volume of fluid with a local (not the lower approach velocity) U_j passing through the grill. For grill 1, $K = 2$ and for the others $K = 1$. These are standard design guide values for grills of this configuration.

Fans 1 and 2 are modelled using quadratic momentum sources of the following form:

$$E_i = C_0 + C_1 U_j + C_2 U_j^2 \tag{14}$$

where E_i is the energy input per unit volume, U_j is the local normal velocity and the constants C_0, C_1 and C_2 are given in Table I. These constants are calculated by making least square fits to manufacturer's data. For fan 1 measurements are made for an input voltage of 15 V. However, data is only available for inputs of 12 and 13.8 V. Therefore, linear extrapolation is used. Fan 2, is 50% obstructed. To account for this, based on tests carried out by the fan manufacturer, a loss coefficient of $K = 1$ is used. For LES-type simulations, at planes where fans are located stochastic forcing to introduce turbulence is tested. However, this is found to have little influence on results.

The Figure 1 domain size is $L = 0.75\,\text{m}$, $H = 0.64\,\text{m}$ and $W = 0.2\,\text{m}$ in the x, y and z directions, respectively. A $105(x) \times 99(y) \times 51(z)$ non-uniform grid is used for all computations. At first off-wall nodes, the average $y^+ \approx 2$. Except for k-l/ILES and DES computations, wall distances are obtained from a Poisson equation. For DES the Eikonal is tried. The k-l/ILES distances are generated by solving Equation (9). For zonal URANS EASM predictions, near walls Wolfshtein's k-l model is used. The interface between the k-l and the EASM is set at $y^*_{\text{int}} = 60(y^* = \rho y C_\mu^{1/4} k^{1/2}/\mu)$.

Table I. Fan constants.

	C_0 (J/m^3)	C_1 (J s/m^4)	C_2 (J s^2/m^5)
Fan 1	59	−12	1.1
Fan 2	59.5	−12.5	1

The flow equations are solved using a standard LES suitable staggered grid finite volume code [13]. Second order central differences are used to discretize the convective and diffusion terms. At walls second order backwards differences are used. For the Crank–Nicolson scheme a one legged temporal discretization is used. By the method of lines we can express the equations to be solved as ordinary differential equations of the following form:

$$\frac{\partial \phi}{\partial t} = f(\phi) \tag{15}$$

With a two legged approach application of the Crank–Nicolson scheme to the above gives

$$\frac{\partial \phi}{\partial t} = \frac{f(\phi^{\text{old}}) + f(\phi^{\text{new}})}{2} \tag{16}$$

where the 'old' and 'new' superscripts represent time levels. For a one legged discretization

$$\frac{\partial \phi}{\partial t} = f\left(\frac{\phi^{\text{old}} + \phi^{\text{new}}}{2}\right) \tag{17}$$

Of course, for a linear function the above two expressions are identical. However, since non-linear equations are here being solved differences will arise. For the NSE $f(\phi\phi)$-type terms occur in the convective terms. To add dissipation, using the one legged discretization we express these terms as $f(\phi^{\text{new}}(\phi^{\text{new}} + \phi^{\text{old}})/2)$. Hence, we include a small dissipative first order fully implicit element. Furthermore, source terms introduced by the fans and grills are discretized fully implicitly. Also, since for incompressible flow the pressure varies instantaneously, the pressure gradient at the new time level is used. Hence, the temporal discretization contains the dissipative element given below:

$$\frac{\partial \phi}{\partial t} = \frac{f[\phi^{\text{new}}(\phi^{\text{old}} + \phi^{\text{new}})]}{2} \tag{18}$$

This will drain turbulence from the resolved larger scales appearing (when using the modified equation approach) as dissipative terms.

3. RESULTS AND DISCUSSION

For mean velocity profiles and turbulence intensities comparisons are made with the LDA measurements of Tucker and Pan [13]. These are available at the six profiles shown in Figure 2. These measurements have an estimated uncertainty of ±5%. Velocities are normalized by the average axial velocities of the two fans ($U_0 \approx 4.5\,\text{m/s}$). Heat transfer comparisons are made along the heated surface centreline in the x direction. The measured Nusselt number error is ±5% [21].

3.1. LES/URANS zones and resulting flow fields

Figure 3 gives contours identifying RANS and LES regions at around the mid x–y plane for the LNS, k-l/ILES and the S–A-based DES. For the k-l/ILES and DES for clearer observation the interface distance has been exaggerated. For DES this is achieved by taking $C_{\text{DES}} = 1.3$. For the k-l/ILES $y^+_{\text{int}} = 100$. This is about three times the value used in later simulations. The

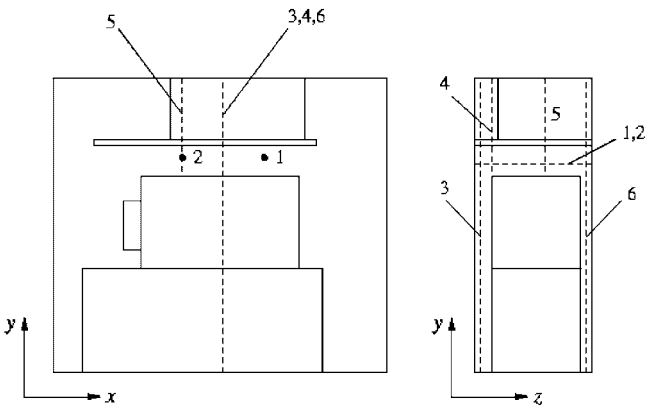

Figure 2. Positions of six profiles investigated.

k-l/ILES distances have been generated solving the HJ Equation (9) as outlined in Tucker [7] with $\varepsilon_0 \approx 0.1$ and $\varepsilon_1 = 0$. The Laplacian in this blends the (U)RANS to the very different ILES turbulence length scale. The general interface nature is similar to that for k-l/LES, but with ILES the length scale drop is much more severe. For the DES the hyperbolic natured Eikonal equation is used (Equation (9) with $\varepsilon_0 = \varepsilon_1 = 0$). This propagates a front from the solid surfaces. The front propagation naturally terminates on reaching the LES filter scale. Except for LNS, dark areas represent the (I)LES region and the lighter gives the URANS zone. In the LNS, the light dark area is mostly URANS and the light zones ($\alpha < 1$) are LES.

As can be seen, for the LNS and DES the interfaces are irregular (if an instantaneous local wall shear stress value is used, it is also irregular for the k-l/LES—hence, this approach is not recommended). This is to be expected. Via Equation (7) instantaneous values decide the LNS interface. For DES it is controlled by the irregular grid. Compared with the other hybrid methods used here, LNS and DES are both found difficult to converge. This is mostly attributed to the irregular interfaces. Also, for LNS, solving one more transport equation for ε detracts from convergence. Although the S–A URANS model proved stable, DES was impossible to converge for the current complex geometry case. Therefore, DES results cannot be presented here. The lower modelled viscosity for DES, relative to LNS, is likely to be a key aspect preventing convergence. Notably, the k-l/ILES gives a smoother interface and hence sensible LES boundary conditions.

Figure 4 shows instantaneous streamlines at mid x–y plane from the k-l/ILES, k-l/LES (at $y^+_{\text{int}} = 30$), Yoshizawa LES, LNS and k-l/EASM. Massive separation (especially in the vicinity of the heated surface), numerous vortex structures and strong streamline curvature can be seen. Comparison of the plots suggests that the k-l/(I)LES and LES capture more small-scale flow activity than the URANS k-l/EASM and LNS.

In the channel like region, containing Profiles 1 and 2 (see Figure 2) all models, except for the LNS, give a significant backwards mean U velocity ($U/U_0 \approx 2$). However, for LNS the flow in this channel is considerably lower ($u/U_0 \approx 0.1$) constituting a significant qualitative flow solution difference.

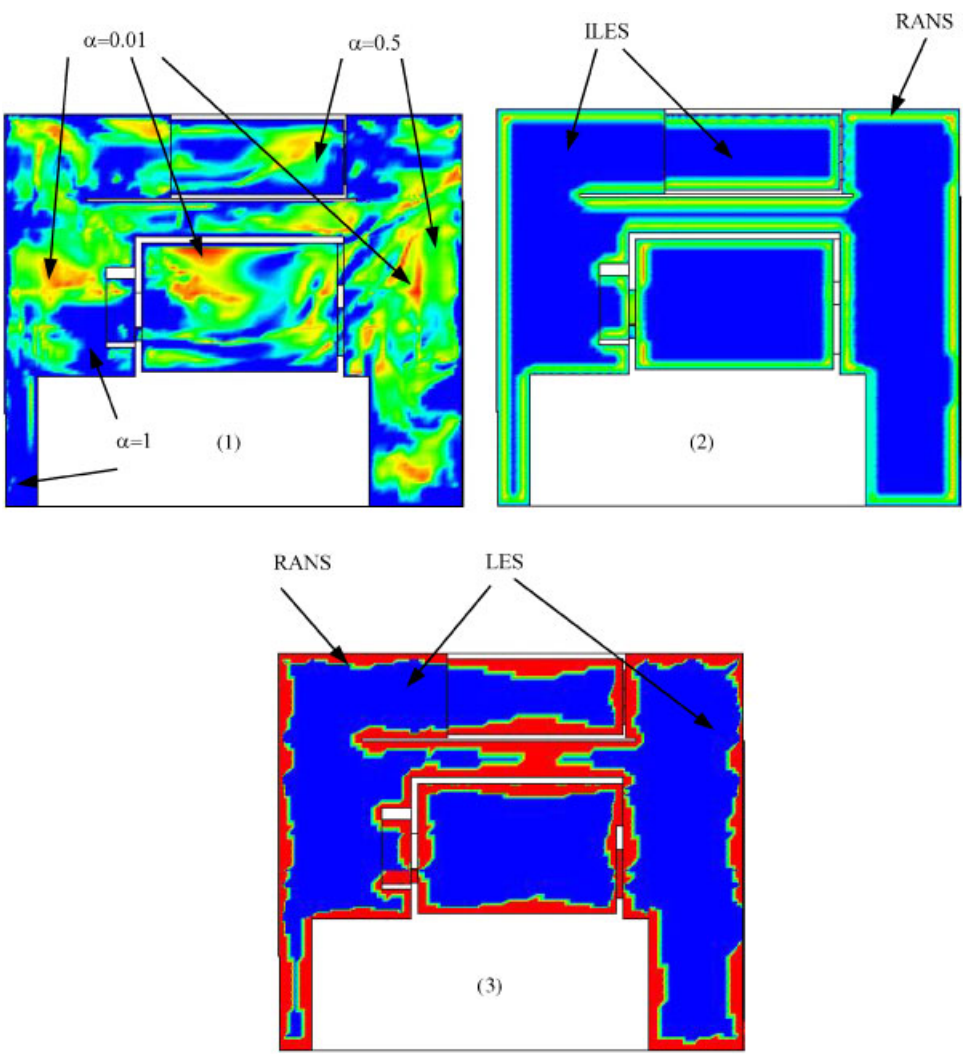

Figure 3. Contours of RANS and (I)LES regions around mid x–y plane: (1) for LNS; (2) for k-l/ILES; and (3) for DES.

The average turbulent viscosity, integrated over the complete domain, for the k-l/ILES, LNS, k-l/LES ($y^+_{\text{int}} = 30$), Yoshizawa LES and k-l/EASM is 7.7e^{-7}, 1.3e^{-3}, 1.4e^{-4}, 7.1e^{-5} and 1.8e^{-3} kg/m s, respectively. Analysis shows, consistent with Reference [14], resolved unsteadiness (averaged over Profiles 1–6) varies inversely with the average turbulent viscosity.

Figure 5 compares U-velocity distributions for Profiles 1–6 and the following models: k-l/ILES, k-l/LES (fixed and dynamic interface) and the k-l/EASM. A qualitative LNS flow difference was noted above and hence due to poor quantitative accuracy LNS results are not shown. This aspect is discussed further later. Spatial coordinates are normalized by the maximum system dimension in each direction. The symbols represent the measurements.

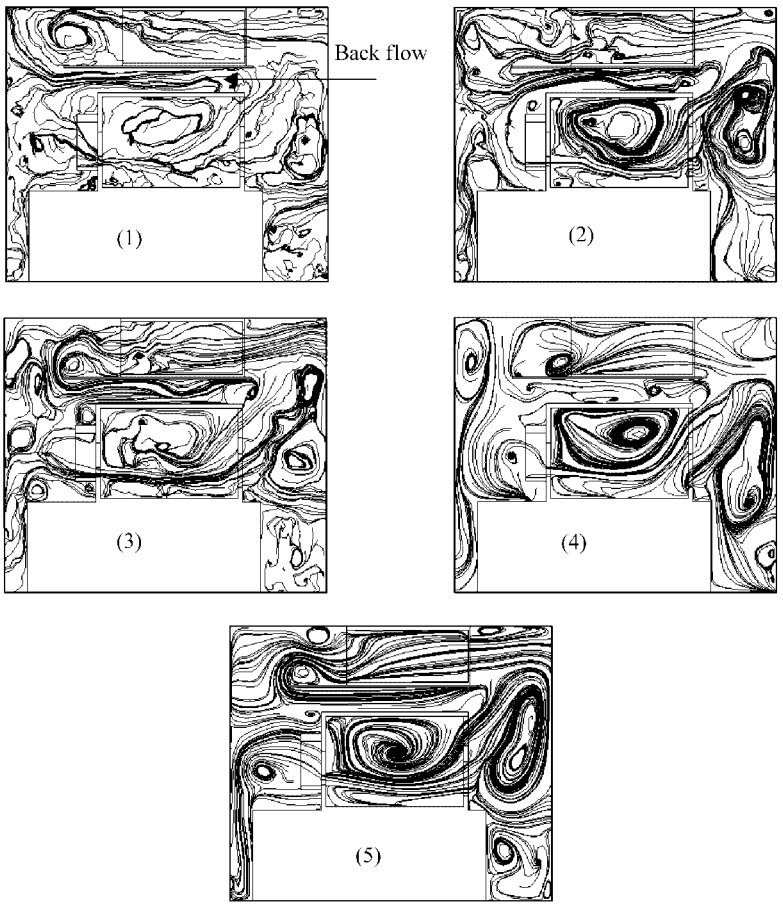

Figure 4. Mid x–y plane instantaneous streamlines from the k-l/ILES (1), k-l/LES (2), LES (3), LNS (4) and k-l/EASM (5).

Except for the k-l/ILES, all models give similar results for all six profiles. It can seen that models can predict the correct trends for some measurement profiles, but not in others. This can also be observed in Figure 6, giving turbulence intensity (T_i) distributions.

To more immediately compare model performances quantitatively, percentage errors for each profile and model are considered using equations (12). Results are summarized in Tables II and III, where the '+' and '−' symbols represent under- and over-predictions, respectively. Table II errors for U suggest that although each model does not perform consistently for all profiles, except for the LNS, all other models generally produce similar velocity accuracies with the same velocity under-prediction bias. Table III shows that the Yoshizawa LES gives the lowest average T_i error. If modelled fluctuations are considered, it would be expected that the difference between the zonal k-l/LES and LES would be smaller. This is because with the k-l/LES, the k-l RANS is strongly used in the near-wall regions. This modelled component is convected and diffused away from walls. Hence, the modelled parts have more influence

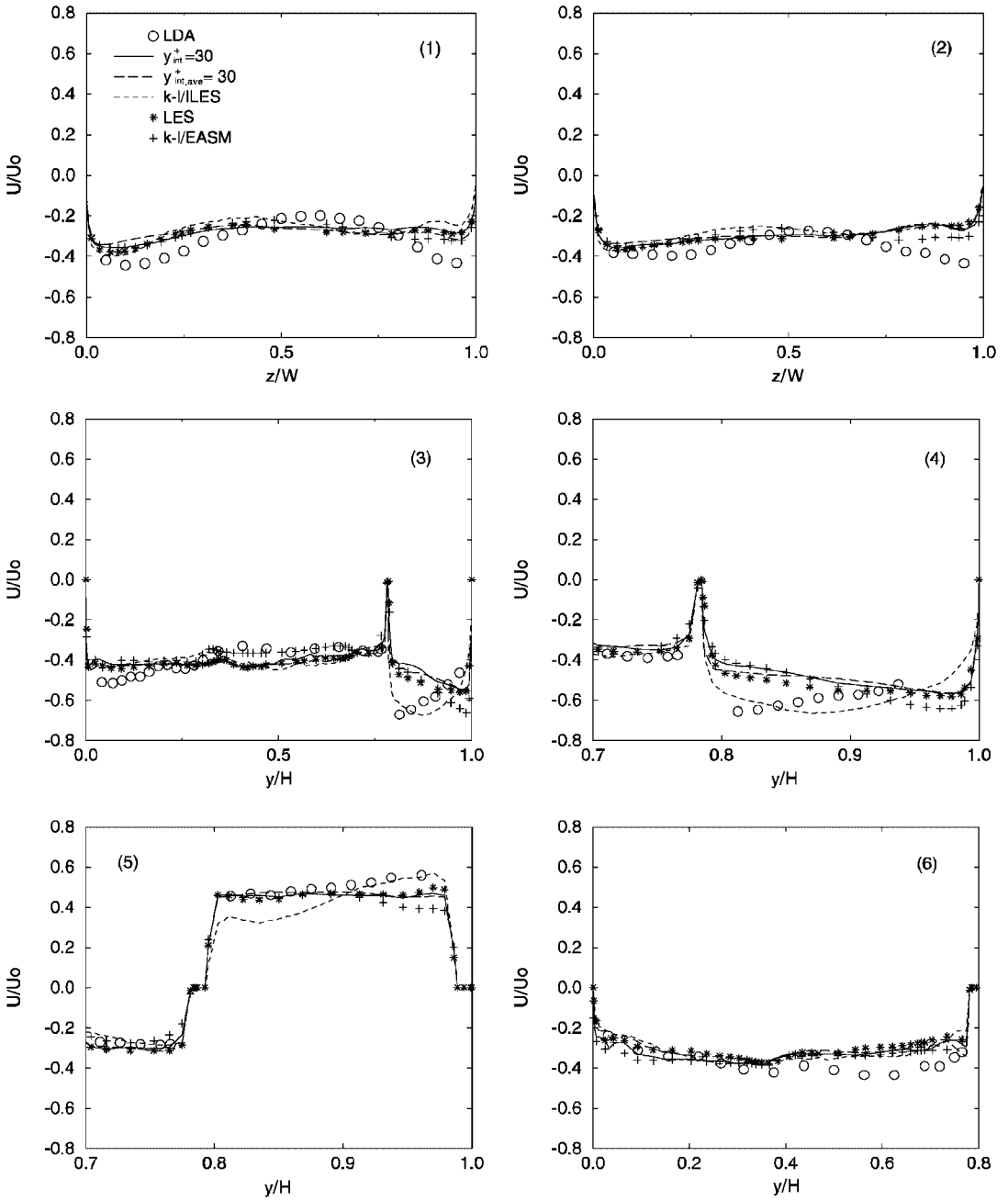

Figure 5. Time-mean U-velocity distributions for Profiles 1–6.

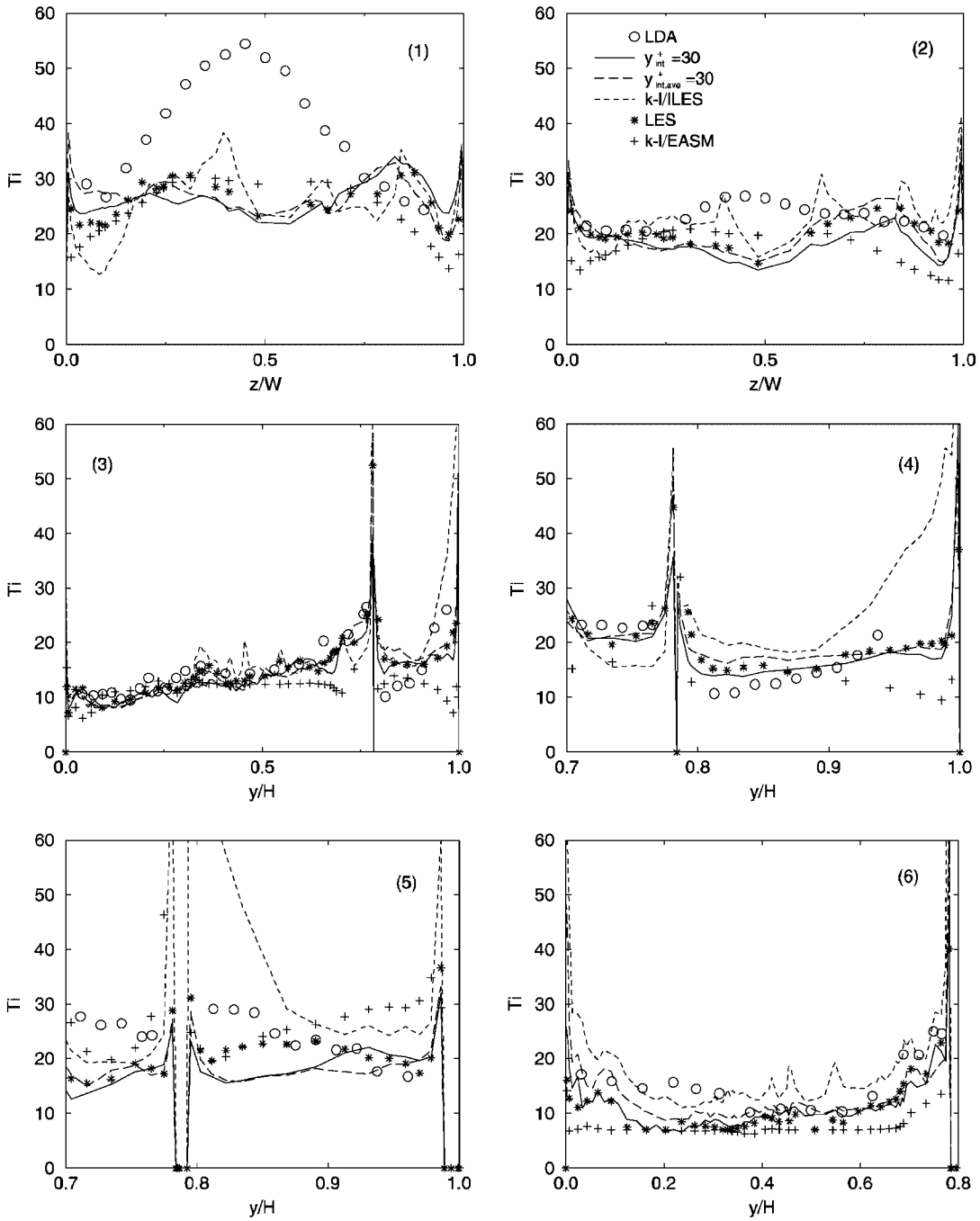

Figure 6. Turbulence intensity distributions for Profiles 1–6.

Table II. Percentage errors (%) in velocity.

Model	Profile 1	Profile 2	Profile 3	Profile 4	Profile 5	Profile 6	Average
k-l/ILES	−23	−19	−12	− 9	−12	−16	−15
k-l/LES ($y^+_{\text{int}} = 30$)	−21	−16	−14	−16	−8	−15	−15
k-l/LES ($y^+_{\text{int,ave}} = 30$)	−22	−19	−14	−16	−8	−16	−16
Yoshizawa LES	−21	−16	−14	−14	−9	−17	−15
k-l/EASM	−17	−14	−13	−17	−11	−15	−15

Table III. Percentage errors (%) in turbulence intensity.

Model	Profile 1	Profile 2	Profile 3	Profile 4	Profile 5	Profile 6	Average
k-l/ILES	−36	−16	−19	+37	+37	+19	+27
k-l/LES ($y^+_{\text{int}} = 30$)	−37	−24	−17	+14	−32	−27	−25
k-l/LES ($y^+_{\text{int,ave}} = 30$)	−34	−19	−17	+17	−30	−19	−23
Yoshizawa LES	−35	−17	−14	+13	−21	−28	−21
k-l/EASM	−32	−22	−22	−24	−26	−49	−29

on the flow in the k-l/LES than in the LES. The k-l/ILES gives a larger average error than the k-l/LES but significantly, unlike all other methods, the T_i error is now positive. Hence, it would seem that the LES-type solutions have too much dissipation of resolved energy and the zonal ILES too little. Also from Table III, it can be seen that the LES-related approaches improve intensity predictions compared to the URANS k-l/EASM result.

It should be mentioned that the LNS performs poorly and in many places gives more than 50% average errors. Even for the case of a simple empty two-dimensional box with a heated sidewall (see Reference [11]), and marginally more complex geometries [22] the question of solution uniqueness can be fairly vexing. Shyy [12] also grapples with this problem for simulations of essentially a simple bifurcating duct, finding two distinct solutions. Similar uniqueness issues occur with multi element airfoil configurations. For these a controlling factor is where peaks in turbulence energy, produced by upstream elements, strike the faces of the downstream elements (see Reference [23]). For the current system, experimental evidence suggests the flow character can perhaps depend on the external environment, i.e. the location of the unit in a room. The poor LNS results could in part be attributed to the LNS model triggering a solution of a slightly different character to that given by the other models. Further possible reasons for discrepancies of the LNS and other models are given later.

3.2. Heat transfer results

Figure 7 shows time-mean local Nusselt number Nu_x along the heated surface centreline in the x direction for all the models examined, where x_0 represents the starting point of the heater. The local Nusselt number is defined as $Nu_x = (x - x_0)q/(k(T_s - T_{\text{ref}}))$, where q is the measured convective heat flux, T_s and T_{ref} surface and reference (the location of the reference point is located just upstream of the heater) temperatures. The symbol k is now used to represent the thermal conductivity of air. It is found that the LES-related approaches under-predict Nu_x especially the LES. The k-l/ILES and k-l/LES approaches predict similar Nu_x

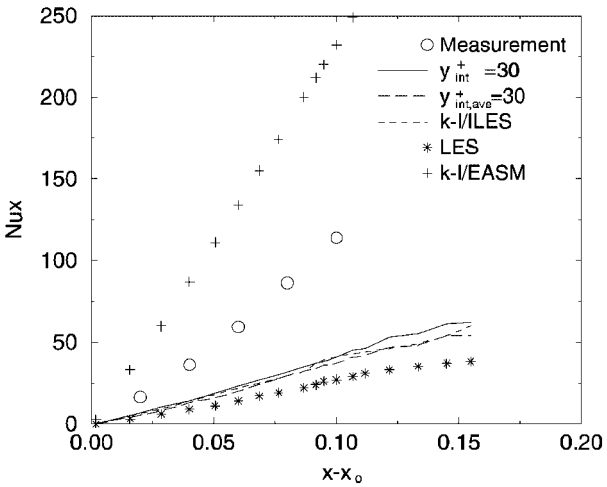

Figure 7. Local Nu_x distributions at the heater surface centreline.

distributions. The k-l/EASM over-predicts Nu_x. However, it should be noted that when used in a high Reynolds number form on a coarser grid the EASM gives impressive agreement [21]. Nevertheless, since the one-dimensional stationary flow wall functions are totally inappropriate for the separated, highly unsteady and three-dimensional heated flow region this result must be regarded as fortuitous and hence is not shown. It might be expected that the added resolved turbulence activity for the less dissipative k-l/ILES approach would yield the highest heat transfer levels for the LES-related methods. However, this is not so. Instead it is k-l/LES with the dynamic interface. It seems possible that the interaction of the strongly time varying interface properties for this approach excites the near wall flow hence increasing heat transfer. However, if this is the case the improved heat transfer is occurring for non-ideal reasons. It is interesting to note past LES approaches (see Reference [24]) and the recent work of Piomelli *et al.* [25] use near wall stochastic forcing. The dynamic interface might, in a crude sense, be akin to this.

Clearly, unlike for the flow field, for Nu_x all models show extremely large errors. However, perhaps this is not too surprising. The high resolution simulations of Chung and Tucker [10], just focusing on a sharply turned flow region, show a 500% change in Nu_x can be induced by small upstream flow perturbations. For the complex Figure 1 geometry there are, in addition to the substantial turbulence modelling errors (especially for heat flux modelling), also significant problem definition issues, i.e. questions on the impact of how well losses introduced by grills and also the energy input from fans are modelled. The latter, in practice, introduce significant flow unsteadiness and swirl. Also, the lower fan shown in Figure 1 is significantly obstructed by a casing component and consequently a characteristic curve correction had to be specially produced by the fan manufacturer. The problem definition questions, combined with experimental, grid dependence and turbulence model errors could easily account for the complex geometry Nu errors and also the velocity and turbulence intensity errors. Another key question, as noted earlier, is solution uniqueness. Electronic systems flows are especially complex with many flow inlets and outlets and hence the potential for multiple solutions is

perhaps significant. This is another aspect worthy of future exploration. Local grid refinement studies were not successful in improving Nu_x prediction. This needs to be further explored.

4. CONCLUSIONS

The k-l/(I)LES, DES, LNS and LES approaches were applied to a complex electronics geometry, non-isothermal flow. Comparisons were made with measurements and a k-l/EASM simulation. Differential distance function equations, including the Eikonal and Hamilton–Jacobi, were used to economically and conveniently assist with the modelling of turbulence length scales. The Hamilton–Jacobi was shown to be especially compatible with the zonal RANS–ILES approach and the Eikonal with DES. For the ILES, the one legged temporal discretization was used to drain turbulence. Generally, all models investigated gave similar the time-mean velocity predictions, with around a 15% error, based on the same relatively coarse grid employed. The LES-related methods gave marginally more accurate turbulence intensities than the URANS k-l/EASM. However, with the exception of the zonal ILES–RANS method, turbulence intensities were under-predicted by around 25%. The LNS method performed especially poorly with mean velocity errors in excess of 50%. This might be attributed to solution non-uniqueness issues. DES solutions could not be converged. This is partly attributed to the grid controlled irregular interface.

Heat transfer results were poor (circa 100% errors). However, it is perhaps worth noting that most established heat transfer measurement data is based on logarithmic scalings. The k-l/EASM model over-predicts heat transfer and the others under-predict, especially the pure LES. The increased flow activity arising from use of the less dissipative ILES element did not significantly improve the predicted heat transfer. However, the added flow activity introduced by the use of a dynamic LES–RANS interface was found helpful. Since the arising interface is highly irregular this approach is not recommended.

ACKNOWLEDGEMENTS

The current work was carried out in support of EPSRC project GR/N05581. This funding is gratefully acknowledged.

REFERENCES

1. Boris JP, Grinstein FF, Oran ES, Kolbe RL. New insight into Large eddy Simulation. *Fluid Dynamics Research* 1992; **10**:199–228.
2. Grinstein FF, Fureby C. Recent progress on MILES for high Reynolds number flows. *ASME Journal of Fluids Engineering* 2002; **124**:848–861.
3. Spalart PR, Jou WH, Strelets M, Allmaras SR. Comments on the feasibility of LES for wings, and on a hybrid RANS/LES approach. *First AFOSR International Conference on DNS/LES in Advances in DNS/LES*, 1997; 137–147.
4. Davidson L, Peng SH. A hybrid LES–RANS model based on a one-equation SGS model and a two-equation k-Ω model. In *Proceedings of the 2nd International Symposium on Turbulence and Shear Flow Phenomena*, Kasagi N *et al*. (eds), 2001; 175–180.
5. Temmerman L, Leschziner MA, Hanjalic K. A-priori studies of a near-wall RANS model within a hybrid LES/RANS scheme. *Engineering Turbulance Modelling and Experiment* 2002; **5**:317–326.
6. Tucker PG, Davidson L. Zonal k-l based Large Eddy simulations. *Computers and Fluids* 2004; **33**:267–287.
7. Tucker PG. Novel MILES computation for jet flows and noise. *International Journal of Heat and Fluid Flow* 2004; **25**(4):625–635.

8. Batten P, Goldberg U, Chakravarthy S. LNS—an approach towards embedded LES. *AIAA Paper*, *AIAA-2002-0427*, 2002.
9. Speziale CG. Turbulence modelling for time-dependent RANS and VLES: a review. *AIAA Journal* 1998; **36**(2):173–184.
10. Chung YM, Tucker PG. Numerical studies of heat transfer enhancement in laminar separated flows. *International Journal of Heat and Fluid Flow* 2004; **25**:22–31.
11. Henkes RAW. Natural-convection boundary layers. *Ph.D. Thesis*, Technical University Delft, Netherlands, 1990.
12. Shyy W. A numerical study of annular dump diffuser flows. *Computer Methods in Applied Mechanics and Engineering* 1985; **53**:47–65.
13. Tucker PG, Pan Z. URANS Computation for a complex internal isothermal flow. *Computer Methods in Applied Mechanics and Engineering* 2000; **190**:1–15.
14. Tucker PG, Liu Y, Chung YM, Jouvray A. Computation of an unsteady complex flow using novel non-linear turbulence models. *International Journal for Numerical Methods in Fluids* 2003; **43**(9):979–1001.
15. Gatski TB, Speziale CG. On explicit algebraic stress models for complex turbulent flows. *Journal of Fluid Mechanics* 1993; **254**:59–78.
16. Yoshizawa A. Bridging between eddy-viscosity-type and second-order models using a two-scale DIA. *Proceedings of the 9th International Symposium on Turbulent Shear Flow*, Kyoto, 1993; 23.1.1–23.1.6.
17. Wolfshtein M. The velocity and temperature distribution in one-dimensional flow turbulence augmentation and pressure gradient. *International Journal of Heat and Mass Transfer* 1969; **12**:301–318.
18. Spalart PR, Allmaras SR. A one-equation turbulence model for aerodynamic flow. *La Recherche Aerospatiale* 1994; **1**:5–21.
19. Smagorinsky J. General circulation experiments with the primitive equations. I: the basis experiment. *Monthly Weather Review* 1963; **91**:99–165.
20. Sethian JA. Fast marching methods. *SIAM Review* 1999; **41**(2):199–235.
21. Liu Y. Numerical simulations of unsteady complex geometry flows. *Ph.D. Thesis*, University of Warwick, U.K., 2004.
22. Quere PL, Xin SH, Gadpin E, Daube O, Tuckerman L. Recent progress in the determination of hydrodynamic instabilities of natural convection flows. *Proceedings of the CHT-04 ICHMT International Symposium on Advances in Computational Heat Transfer*, Norway, CHT-04-K4, 2004.
23. Tucker PG, Rumsey CL, Spalart PR, Bartels RE, Biedron RT. Computations of wall distances based on differential equations. *AIAA Journal* 2005; **43**:539–549.
24. Mason PJ, Thomson DJ. Stochastic backscatter in Large-eddy Simulation of boundary layers. *Journal of Fluid Mechanics* 1992; **242**:51–78.
25. Piomelli U, Balaras E, Pasinato H, Squires KD, Spalart PR. The inner–outer layer in Large-eddy Simulations with wall layer models. *International Journal of Heat and Fluid Flow* 2003; **24**:538–550.

